Di-Jet Imbalance A_J
Analysis Note

PAs: Helen Caines, Kolja Kauder, Jörn Putschke

July 6, 2016 version 4.0

Contents

1 Physics Summary and Figures

We present (for the first time at RHIC) the di-jet imbalance

$$A_J \equiv \frac{p_T^{\mathrm{Lead}} - p_T^{\mathrm{SubLead}}}{p_T^{\mathrm{Lead}} + p_T^{\mathrm{SubLead}}} \tag{1}$$

in 200 GeV, HT-triggered, 0-20% Au+Au, compared to HT-triggered p+p data embedded into untriggered 0-20% Au+Au. Jets are found using the anti-k_T algorithm with a resolution parameter of $R = 0.4$. The nominal di-jet selection is done using a constituent cut $p_T^{\mathrm{Cut}} > 2\,\mathrm{GeV}/c$ and requiring $p_T^{\mathrm{Lead}} > 20\,\mathrm{GeV}/c, p_T^{\mathrm{SubLead}} > 10\,\mathrm{GeV}/c$ with an opening angle between leading and sub-leading jet of $\left|\phi^{\mathrm{Lead}} - \phi^{\mathrm{SubLead}} - \pi\right| < 0.4$.

The analysis is then repeated on the events where di-jets where found, but this time relaxing the constituent requirement to $p_T^{\mathrm{Cut}} > 0.2\,\mathrm{GeV}/c$. For these events the matched A_J is calculated using those jets found within $\Delta R < 0.4$ of the original di-jet pair.

1.1 Figure 1

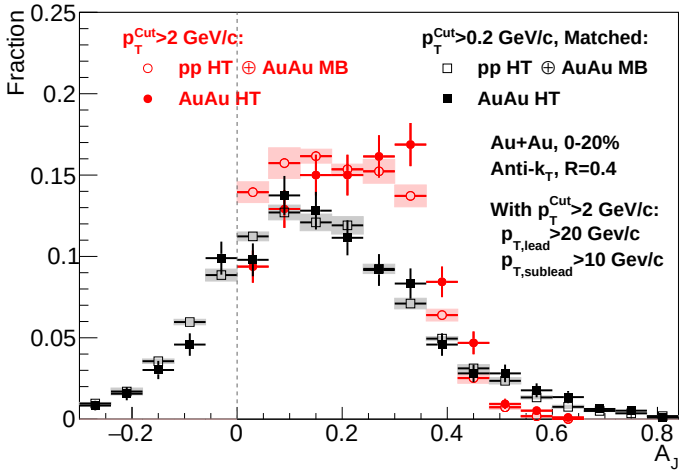

Figure 1: (Color online.) Normalized A_J distributions for Au+Au HT data (filled symbols) and p+p HT $\oplus$ Au+Au MB (open symbols). The red data points are for jets found using only constituents with $p_T^{\mathrm{Cut}} > 2$ GeV/c and the black ones for matched jets found using constituents with $p_T^{\mathrm{Cut}} > 0.2$ GeV/c. In all cases $R = 0.4$.

The A_J distributions for the above selections are shown in Figure 1. All Figures includes a dashed line at 0 to guide the eye.

Observations:

- With a $2\,\mathrm{GeV}/c$ constituent cut (red data points), the A_J distribution shows significantly *more imbalanced di-jets* in central Au+Au than in the embedded p+p reference. The p-value, calculated Kolmogorov-Smirnov test on the unbinned data (only statistical uncertainties were included), is found to be negligibly small, indicating a statistically significant difference between the two distributions.
- For matched di-jets with a $0.2\,\mathrm{GeV}/c$ constituent cut (black data points), the distributions are found *identical* within uncertainties between Au+Au and embedded p+p, with a p-value around 0.5, indicating that the hypothesis of identical underlying distributions cannot be rejected at any reasonable confidence level.

This observation of significant imbalance in Au+Au that can be restored to the level of p+p within the original jet cone is qualitatively new. A_J measurements at the LHC report missing energy far outside the cone region. It is consistent with expectations from significant bias toward surface bias at RHIC, i. e. the di-jet selection here may lead to almost tangential di-jets that experience some medium interaction but not to the point where the energy is completely dissipated ("lost").

1.2 Figure 2

The increase in background fluctuations for the low constituent p_T-cut would naturally lead to an artificial balance unrelated to potential modifications in the jet fragmentation. We estimated this effect firstly by embedding the Au+Au HT di-jets reconstructed with a constituent p_T-cut $p_T > 2$ GeV/c (corresponding to the closed red markers in Figure 1) into Au+Au MB events with a low constituent p_T-cut and calculated A_J, hence explicitly not allowing any balance restoration via correlated jet signal constituents (*Random Cone* method (RC)).

In order to account for potential correlations of the di-jets with respect to the reaction plane, we repeated this procedure but embedded into HT events where di-jets where found, at the identical azimuth position but offset in pseudorapidity by $2 \times R$ (*Eta Cone* method (EC)).

The results of both methods are shown in Fig. 2, are compared to the measured matched A_J distribution with a low constituent p_T-cut.

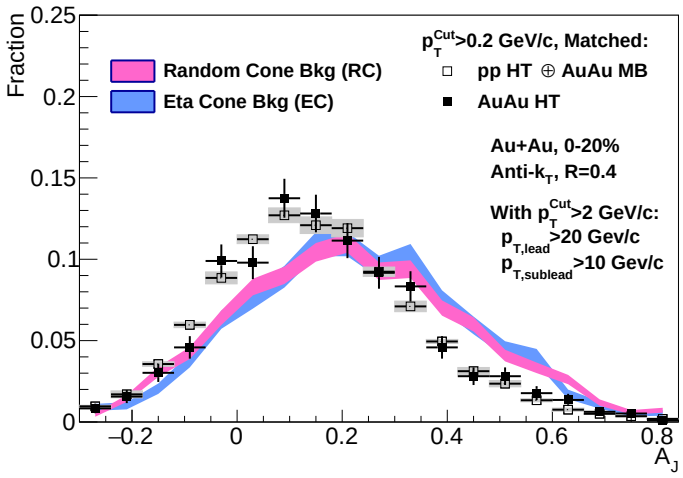

Figure 2: (Color online.) A_J distributions for Au+Au data (filled symbols) and p+p HT $\oplus$ Au+Au MB (open symbols) for low constituent $p_T^{\rm Cut}$ di-jets from Fig. 1 compared to A_J distributions calculated assuming the RC and EC null hypotheses, respectively, shown as colored bands; see the text for details.

Observations:

- It is clear that while background fluctuations contribute some to the rebalancing, they alone cannot account for the observed balance, confirming that the balance is restored via low p_T constituents *correlated to jet production.*

For reference, the p-value (calculated with a χ^2 test in this case) of either RC or EC being identical to Au+Au is less than 10^{-10}, the p-value between RC and EC is 0.2, numerically indicating that the influence of azimuthally correlated background is small.

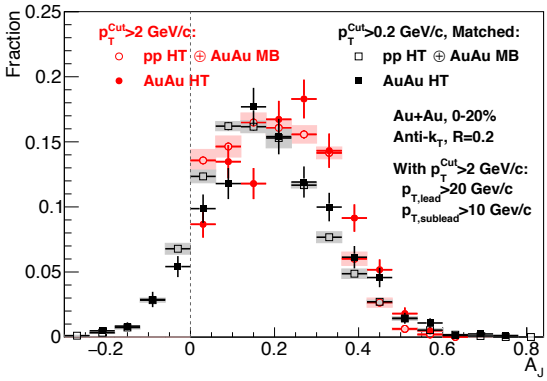

Figure 3: (Color online.) Repetition of the analysis shown in Fig. 1 with a smaller resolution parameter $R = 0.2$. Normalized A_J distributions for Au+Au HT data (filled symbols) and p+p HT $\oplus$ Au+Au MB (open symbols). The red data points are for jets found using only constituents with $p_T^{\text{Cut}} > 2$ GeV/c and the black ones are for matched jets found using constituents with $p_T^{\text{Cut}} > 0.2$ GeV/c.

1.3 Figure 3

To assess whether the observed softening of the jet fragmentation is accompanied by a broadening of the jet profile, the di-jet imbalance measurement was repeated with a resolution parameter of $R = 0.2$, the result is shown in Figure 3.

Observations:

- As expected, Au+Au di-jets are more imbalanced than the p+p reference for a high p_T constituent cut and a narrower cone cut $R = 0.2$.
- The matched low p_T constituent cut A_J measurements however demonstrate that a resolution parameter of $R = 0.2$ is *not sufficient* to restore the Au+Au imbalance (solid black markers) to the embedded p+p reference (open black markers), also expressed in the calculated p-value below 2^{-5}.

2 Analysis Details

2.1 Data Set

Data in this analysis are from Run 7 Au+Au collisions and Run 6 p+p collisions at $\sqrt{s_{NN}} = 200$ GeV. The following parameters are used in the event and track selections:

- 0-20% centrality in Au+Au (gRefMult >268 [1])
- $|v_z| < 30$ cm
- Track cuts: Fit Points Over Max Points >0.52, DCA <1 cm, Number of Fit Points ≥ 20, $|\eta_{track}| < 1.0$
- 100% hadronic correction is applied to the BEMC towers. Electrons are *not* rejected for this scheme.
- Events containing a track with $p_T > 30$ GeV/c are rejected because of poor momentum resolution. Unphysically high towers are also rejected, and for ease and consistency the same 30 GeV/c cutoff was used. Fig. 4 demonstrates that the effect is all but negligible.

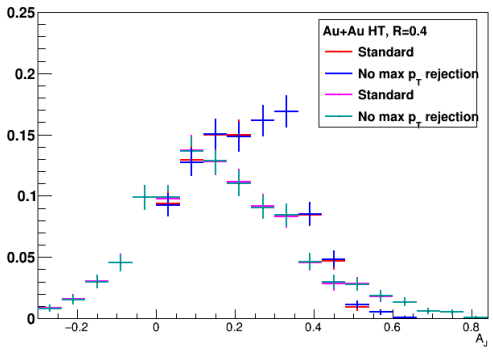

Figure 4: Effect in Au+Au HT for $R = 0.4$ of rejecting constituents above 30 GeV/c.

- Trigger IDs:
  - p+p HT: 117211, 117212, 127212, 127213, 137213 [2]
  - Au+Au HT: 200620, 200621, 200211, 200212, 200220, 200221, 200222 [3]
  - Au+Au MB: 200001, 200003, 200013 [3].

Data	#Events	Luminosity [nb^{-1}]	#Di-jets
p+p HT		11.3	1554
Au+Au HT	4.3M	1.12	992 (in 0-20%)
Au+Au MB	44k (sample)	N/A	N/A

Table 1: Number of events, integrated luminosity, and number of di-jet pairs found with $R = 0.4$ and $p_T^{\text{Cut}} > 2$ GeV/c for the three used data sets.

2.2 Jet Reconstruction

Jets are reconstructed from charged tracks in the TPC and neutral towers in the BEMC using the anti-k_T algorithm in FastJet [4, 5] with resolution parameters $R = 0.4$ and $R = 0.2$. Unless otherwise noted, default parameters are used as set in FastJet release 3.0.3. The axes of the reconstructed trigger jets are required to fall within $|\eta_{jet}| < 1 - R$.

2.2.1 Jet p_T

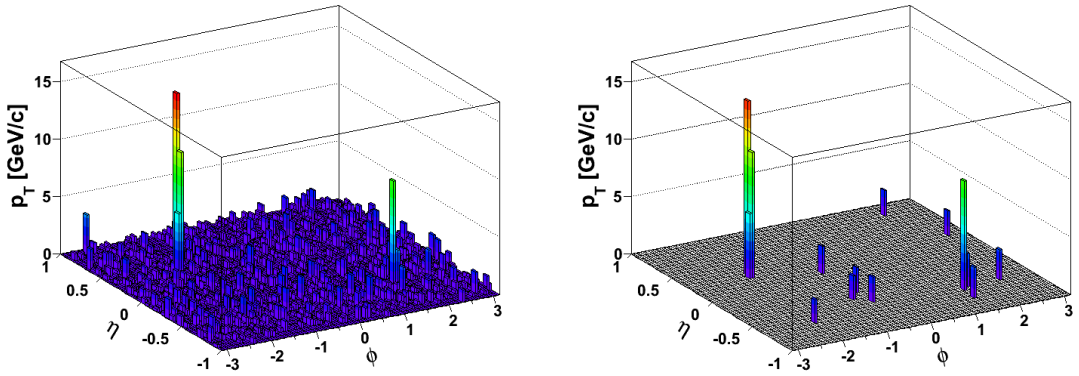

Figure 5: Example di-jet event before (left) and after (right) application of the constituent $p_T^{\text{Cut}} > 2$ GeV/c cut.

The constituent $p_T^{\text{Cut}} > 2$ GeV/c cut greatly reduces the effects of background fluctuations by eliminating the low-p_T heavy-ion background, see Figure 5. For these jets, we therefore directly used

$$p_T^{\text{Jet}} = p_T^{\text{Rec}}. \tag{2}$$

Reconstructed jets using all constituents above 0.2 GeV/c however require background correction. To that end, we follow the procedure in Reference [5], Chapters 7 and 8, and classes provided by the FastJet package. The background density ρ in an event is determined as the median of $p_T^{\text{Jet, Rec}}/A^{\text{Jet}}$ of all but the two leading jets, determined using the k_T algorithm with the same resolution parameter R as in the nominal jet reconstruction. Jet areas A^{Jet} are found using active areas with ghosts out to $|\eta| < 1 + R$.

Areas are constructed in 4-vector form, and jet momenta are then corrected from the raw momenta $p_\mu^{\text{jet,Rec}}$ via subtraction:

$$p_\mu^{\text{jet}} \equiv p_\mu^{\text{jet,Rec}} - \rho A_\mu^{\text{jet}}. \tag{3}$$

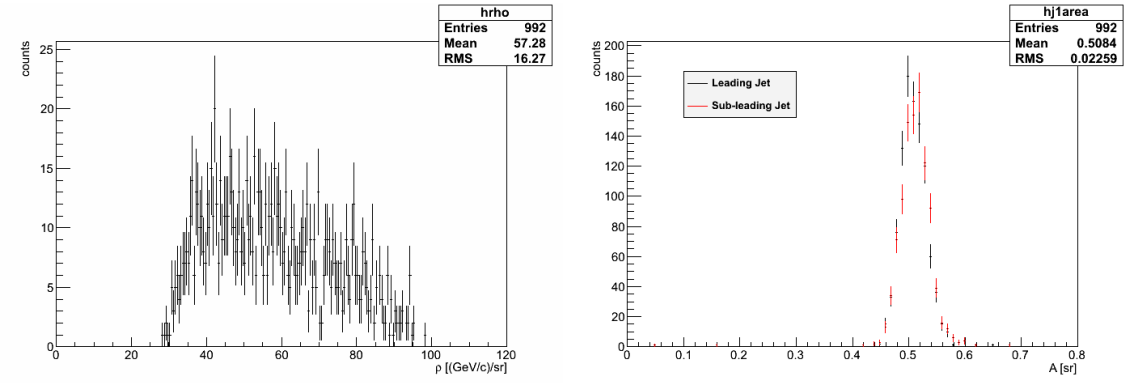

Figure 6: Distributions of ρ (left) and area of leading and sub-leading di-jets (right) in HT Au+Au.

2.2.2 Hadronic Correction

Charged tracks can also leave energy in the calorimeter. To avoid double-counting this energy, we adopted a 100% hadronic correction, where the entire p_T of a track matched to a calorimeter tower is subtracted from that tower's energy. Tower energies are set to zero if they would otherwise become negative via this correction. As an alternative, we tested 30% and 70% correction, as well as the other extreme, the MIP correction, where instead only the minimum ionizing energy is subtracted, as parameterized by

$$\theta \equiv 2\tan^{-1}\eta, \tag{4}$$

$$E_{\mathrm{MIP}} = (0.261\ \mathrm{GeV}/c)\,\frac{1+0.056\,\eta^2}{\sin(\theta)}. \tag{5}$$

The result is compared to the nominal result in Fig. 7. Note that this cross-check was done prior to switching from displaying $|A_J|$ to displaying A_J.

While there is some effect on the shape of the distributions and on the total number of reconstructed di-jets, Au+Au and embedded p+p are affected similarly and the physics remain unchanged. It has been shown previously that the 100% correction provides a better description of the jet p_T spectrum than the MIP correction[6]. Since the key point of this measurement is comparison between Au+Au and embedded p+p, we do not assign a systematic uncertainty based on the MIP correction.

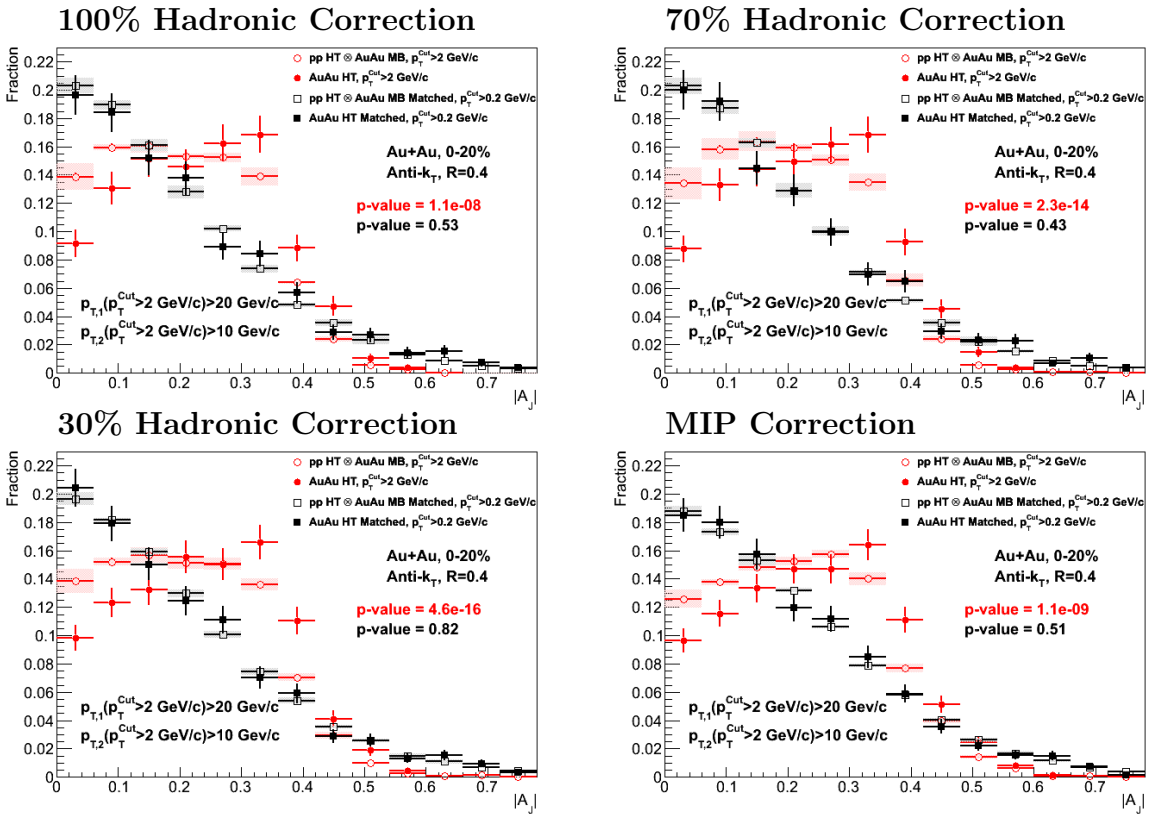

Figure 7: Normalized $|A_J|$ distributions (R=0.4) with varied hadronic correction schemes.

2.3 Embedding

In this analysis, we do not try to correct for detector and background effects via unfolding. Instead we assess these effects by comparing A_J in Au+Au to a reference obtained by embedding p+p HT events into

Minimum Bias Au+Au event randomly selected from the same 0-20% centrality class.

In addition, the null hypothesis that the rebalancing effect for low-p_T constituents is overwhelmingly due to background fluctuations, not correlated yield, is tested with the Random Cone and Eta Cone Method which also rely on embedding, this time of jets found in Au+Au into Au+Au MB or Au+Au HT.

2.3.1 p+p HT ⊕ Au+Au MB Embedding

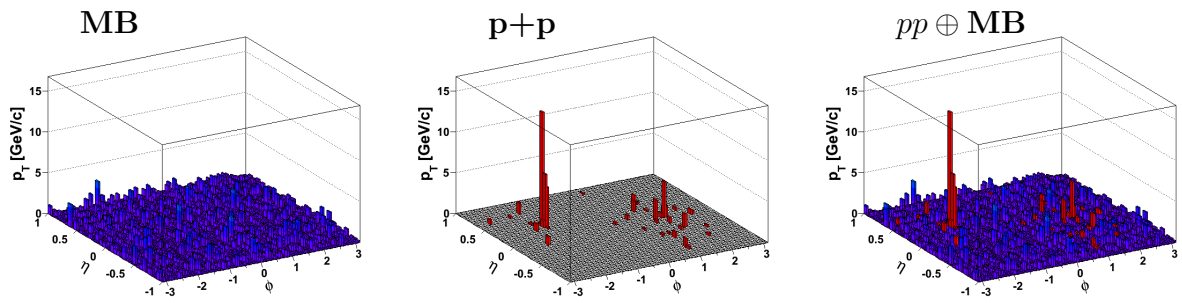

Figure 8: Example of a Au+Au MinBias event, a p+p event with a dijet, and the combination of the two.

As illustrated in Figure 8, p+p events are combined track-for-track and tower-for-tower with 0-20% Au+Au events. Specifically, p+p events were pre-selected to contain at least a $p_T > 10$ GeV/c jet, and a sample of 44k MB Au+Au events (about 14k in 0-20%) was mixed with them, each with six randomly selected events. The spectrum of trigger jets in p+p is shown in Fig. 9. The figure also shows the effect of the Au+Au background and detector effects on the reconstructed p_T for leading $R = 0.4$ jets. About 28% of leading jets are contributed by jets that were originally below the 20 GeVc threshold. Not shown in the figure, this numberis about the same for di-jet pairs (30%).

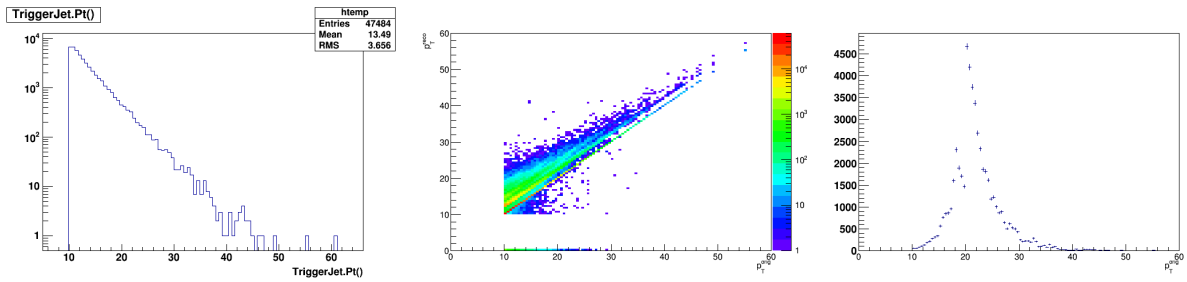

Figure 9: Left: Leading jet spectrum of p+p HT events selected for embedding. Middle: Reconstructed vs. original leading hard-core jet p_T. The band structure is due to the 2 GeV/c cut. Right: Projection over trigger jets selected for the analysis, i.e. $p_T^{\mathrm{Reco}} > 20$ GeV/c. About 28% are contributed by jets that were originally below the 20 GeVc threshold. In all cases $R = 0.4$.

The analysis is then carried out identically on these hybrid events. To avoid pathological situations, events were rejected if the original leading jet in p+p could not be matched to either leading or the sub-leading jet in the hybrid event. Additional details of this embedding technique were explored in the jet-hadron paper [6], and in Alice Ohlsen's thesis [8].

2.3.2 Detector Effects Between p+p and Au+Au

Due to the lower occupancy, track reconstruction efficiency is significantly lower in central Au+Au than in p+p. To account for this difference, charged tracks from the p+p event are randomly discarded during the

embedding process, following the p_T-η-dependent ratio of tracking efficiencies. We used the parameterized efficiency curves for Run6 and Run7 that were obtained for the Jet-hadron paper [6], see Figure 10.

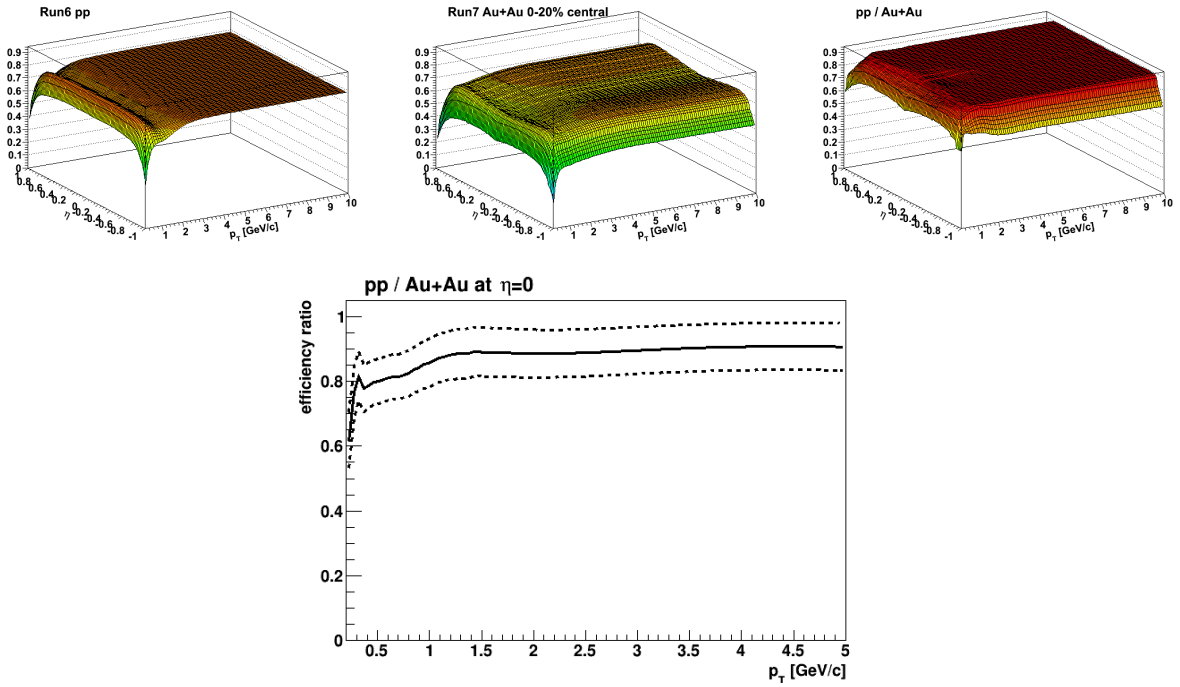

Figure 10: Left: Tracking efficiency in Run6 p+p. Middle: Tracking efficiency in Run7 Au+Au, 0-20% central. Right: Ratio of the two, i.e., the probability that a charged p+p track is kept during embedding. Bottom: Ratio at $\eta = 0$ with the uncertainty shown as dashed lines.

While masked BEMC towers in one data set are removed in the other as well, the tower efficiency in Au+Au is ∼98% that in p+p. In order to reflect this in the Au+Au MB embedding, we randomly rejected 2% of towers in the p+p event.

2.3.3 Au+Au Jets in Au+Au MB/HT Embedding (RC and EC)

This test serves to test whether the red solid (hard core Au+Au) A_J in Figure 1 can be transformed into the black solid curve by adding soft background yield that is not jet-like. To that purpose, we embed di-jets with $p_T^{\mathrm{Cut}} > 2\,\mathrm{GeV}/c$ found in the original analysis into different Au+Au events, and fill them up with random cones. For these tests, we embed di-jets with $p_T^{\mathrm{Cut}} > 2\,\mathrm{GeV}/c$ found in the original analysis into different Au+Au events. Two classes of events to embed into are considered (visualized in Figure 11):

Random Cone: For this method, we use the same Au+Au MB events as in Section 2.3.1. Every event is mixed with six dijets.

Eta Cone: To assess the influence of underlying correlations besides the jet components, in this approach Au+Au HT events with found dijets are used, the test dijets are then embedded at a distance of at least $2R$ in pseudorapidity from the actual jet in the event. Again, six di-jets are mixed with each event.

Note that in either case, no jet-like yield below 2 GeV/c is inside the jet cone; any balance restoration is due to the heavy ion background. Our findings show that though there is a balancing effect (through smearing), uncorrelated as well as only elliptic-flow-like yield is not nearly enough to account for the observed magnitude.

Method For the Eta Cone method, the presence of four jets in the acceptance would impact the jet-finding. Therefore, we instead approximate the result of jet-finding by assuming perfectly spherical jets of radius R, an excellent approximation for leading and sub-leading anti-k_T jets [5]. For simplicity and consistency, this method is used for the Random Cone as well. The di-jet imbalance is then calculated with new p_T^{Jet} values obtained from the original one via

$$p_\mu^{\text{Jet}} = p_\mu^{\text{Jet,Orig}} + \sum_{\Delta R<R} p_\mu^{\text{constituent}} - \rho\pi R^2, \tag{6}$$

where the summation is over all constituents inside the circular "jet" cone, and ρ is obtained as before (in the case of embedding into MinBias, the rejection of the two hardest jets in the calculation of ρ is dropped).

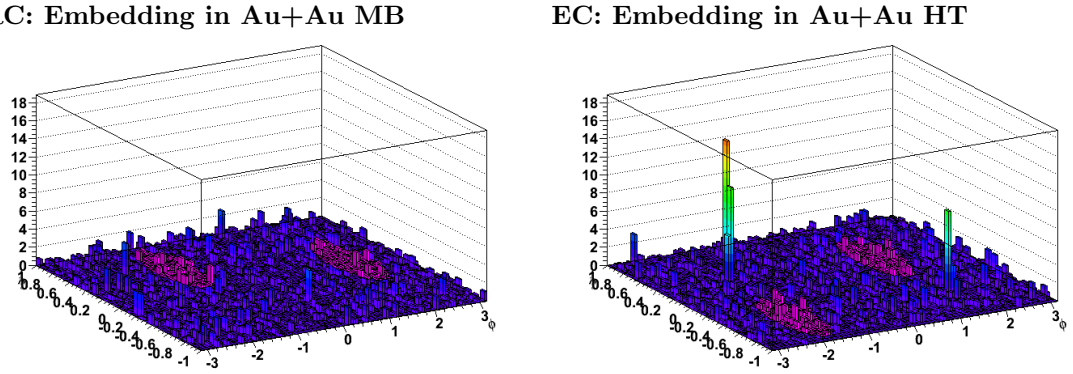

Figure 11: Choices for soft background. Left: Random Cone. Embed into Au+Au MB at the original positions of the di-jet pair to be mixed with. Right: Eta Cone. Embed into Au+Au HT at the positions of the di-jet found in the event, randomly off-set in η to be at least $2R$ away.

3 Systematic Uncertainties

The performance of the TPC and BEMC can vary in different collision systems and over time. As discussed at length in the jet-hadron paper GPC, naïve addition of the standard 5% tracking uncertainty is unreasonable. The difference between the tracking efficiency in Run 4 and Run 7 is approximately 3% (absolute) in the 0-5% centrality bin, so we take this as a conservative estimate of the run-dependence of the tracking efficiency. Since we take embedded pp to be representative of Run7 Au+Au, this uncertainty applies to both Run 6 (p+p) and Run 7 (Au+Au), i.e., it should be applied twice. An additional 4% uncertainty is applied to the AuAu efficiency to account for centrality dependence. In total, the total uncertainty on the efficiency ratio $\varepsilon_{\text{Au+Au}}/\varepsilon_{pp}$ is

$$\frac{\varepsilon_{\text{Au+Au}}}{\varepsilon_{pp}} \times \sqrt{(3\%/\varepsilon_{pp})^2 + (3\%/\varepsilon_{\text{Au+Au}})^2 + (4\%/\varepsilon_{\text{Au+Au}})^2} \tag{7}$$

The ratio is 90% over a wide pT range, and the uncertainty generally about 7%, both figures only deviate at very low p_T, see Fig. 10.

The relative tower efficiency was determined to $98\% \pm 2\%$ [6]. These variations in detector performance were evaluated individually by repeating the p+p HT $\oplus$ Au+Au MB measurements using the upper and lower ends. The full range was used, and the two sources added in quadrature for the systematic uncertainty on A_J in the p+p HT $\oplus$ Au+Au MB embedding reference (shown as colored shaded bands).

3.1 Relative Tracking Efficiency – Systematic Uncertainties

The result of varying the relative tracking efficiency shown in Figure 12.

3.2 Relative Tower Efficiency – Systematic Uncertainties

The result of varying the relative tower efficiency in $98\% \pm 2\%$ is shown in Figure 13.

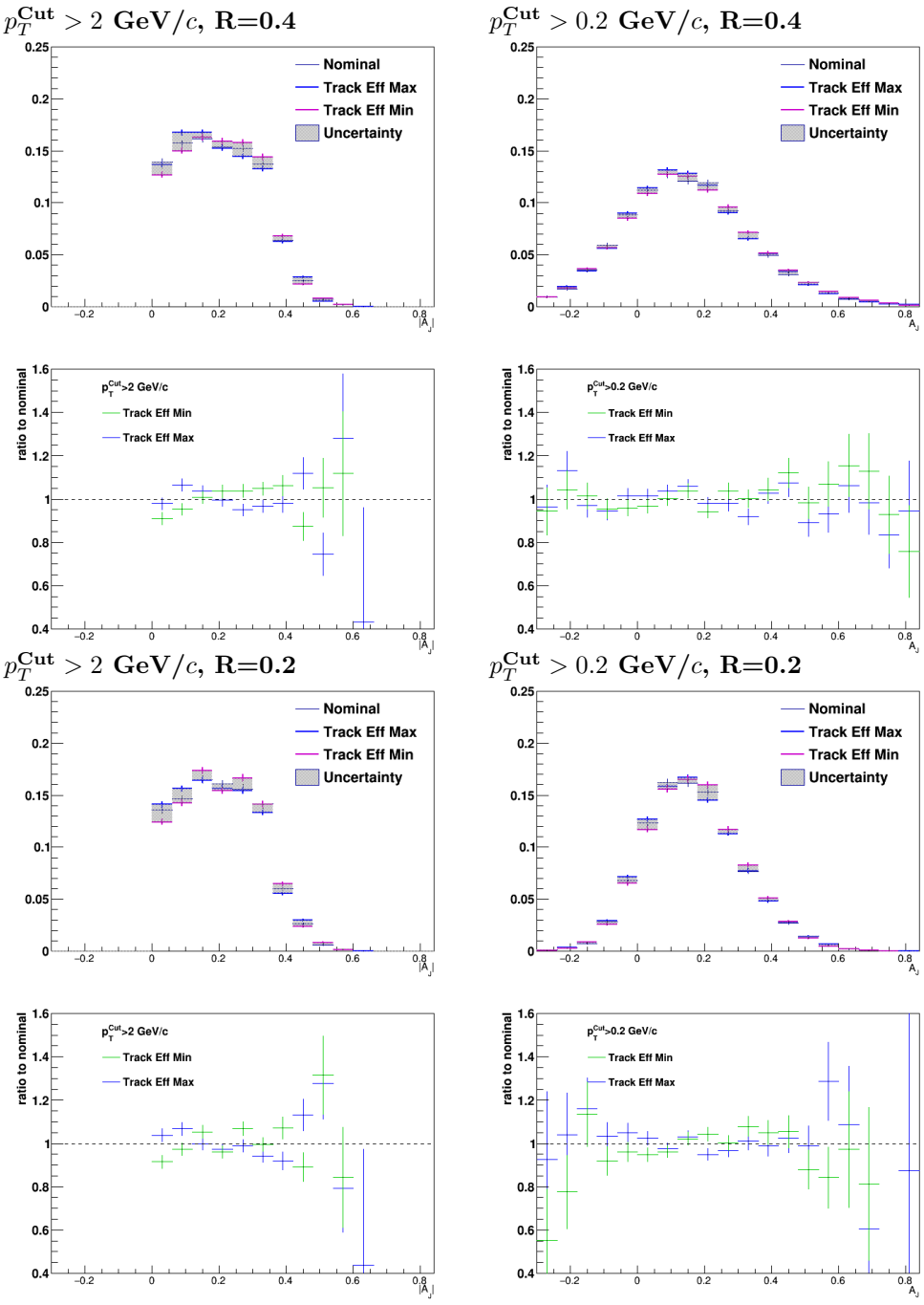

Figure 12: Result of varying the relative tracking efficiency by ±7% in p+p HT ⊕ Au+Au MB embedding for all constituent cut and R combinations.

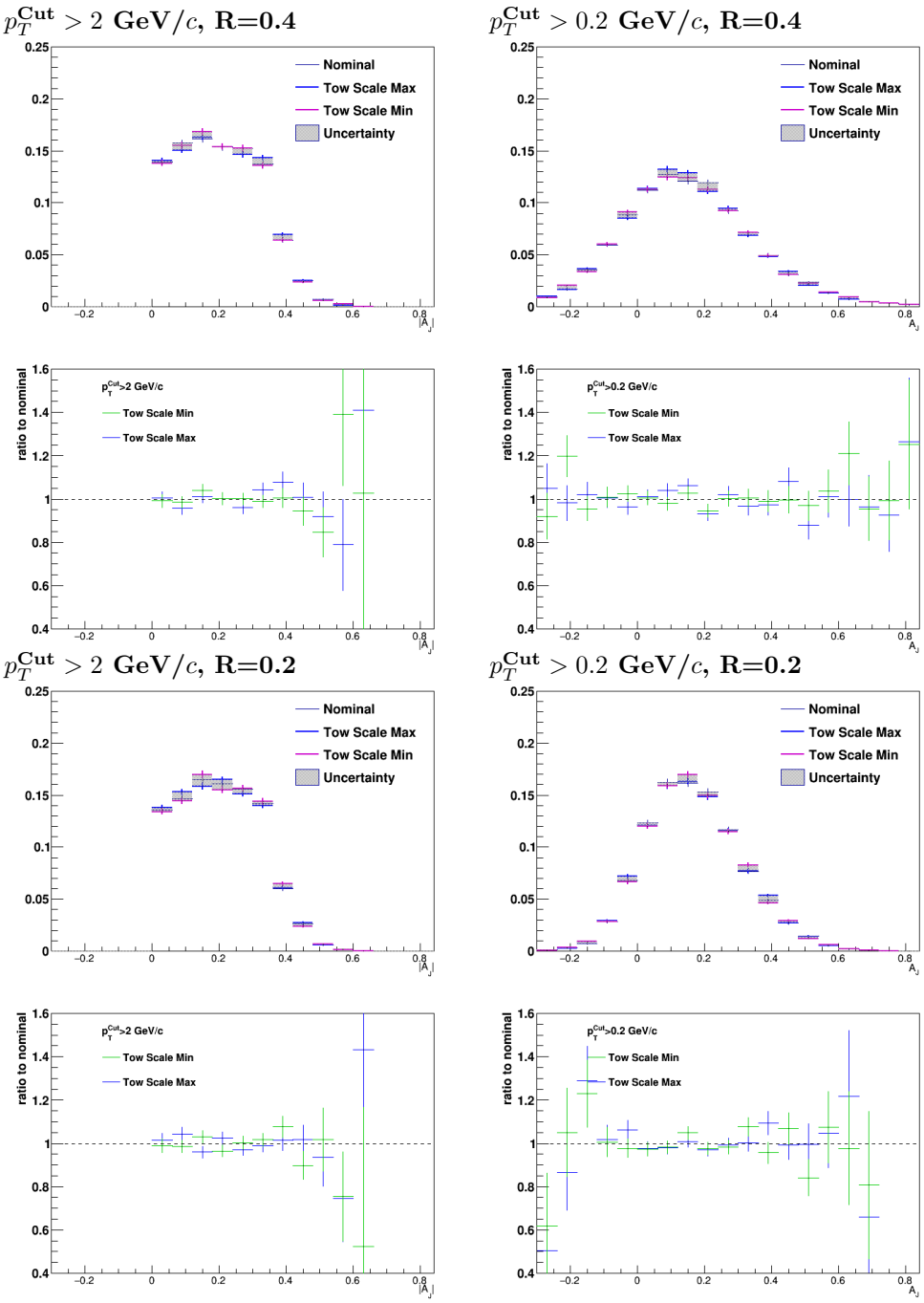

Figure 13: Result of varying the relative tower efficiency by ±2% in p+p HT ⊕ Au+Au MB embedding for all constituent cut and R combinations.

3.3 p-Value

Multiple tests are available to test whether two histograms sample the same distribution. A χ^2-test ulitmately compares two histograms point-for-point, and is less appropriate for the situation here where differences would correspond to bin migrations. It is also sensitive to binning. We therefore use an un-binned Kolmogorov Smirnov (KS) test which is designed to be sensitive to both location and shape [7]. However, as shown in Table 2, the particular choice of χ^2-test, binned, or un-binned KS test does not change the physics message.

R	$\mathbf{p_T^{Cut}}$	**un-binned KS**	**binned KS**	χ^2**-test**
$R = 0.4$	2 GeV/c	**4E-9**	1E-6	4E-7
	0.2 GeV/c	**0.42**	0.41	0.51
$R = 0.2$	2 GeV/c	**1E-8**	4E-6	5E-6
	0.2 GeV/c	**7E-8**	1E-7	1E-16

Table 2: Comparison of p-values obtained with binned tests compared to the nominal un-binned Kolmogorov-Smirnov value.

3.3.1 Systematics on the p-Value

There is significant point-by-point correlation in the systematic uncertainties (cf. the ratios above), and assessing the effect of systematic uncertainties via the quadrature sum is therefore not appropriate. We explored the p-values comparing each of the four variations of tracking and tower efficiency individually in the Table 3. For an estimate of systematic effects we quote the range of minimal and maximal values obtained during these variations, see Table 4.

R	$\mathbf{p_T^{Cut}}$	**un-binned KS**				
		nominal	HighTrack.Eff.	LowTrack.Eff.	HighTow.Eff.	LowTow.Eff.
$R = 0.4$	2 GeV/c	**4E-9**	4E-10	1E-6	1E-7	5E-9
	0.2 GeV/c	**0.42**	0.39	0.6	0.33	0.25
$R = 0.2$	2 GeV/c	**1E-8**	1E-9	3E-7	1E-8	3E-7
	0.2 GeV/c	**7E-8**	3E-7	2E-8	4E-7	8E-8

Table 3: Comparison of (un-binned Kolmogorov-Smirnov) p-values for the four extremes used to assess systematic uncertainty.

R	$\mathbf{p_T^{Cut}}$	**Quoted Range (un-binned KS p-value)**
$R = 0.4$	2 GeV/c	4E-10—1E-6
	0.2 GeV/c	0.2—0.6
$R = 0.2$	2 GeV/c	1E-9—3E-7
	0.2 GeV/c	2E-8—4E-7

Table 4: Resulting p-value ranges quoted in the paper.

Purely as a cross-check, the p-value for the binned variants was recalculated using the systematic uncertainty added in quadrature to the statistical errors. Enlarging error bars will naturally lead to a larger p-value. It still leads to a p-value below 1% (corresponding roughly to three sigma significance) for the question whether the $p_T^{\mathrm{Cut}} > 0.2\,\mathrm{GeV}/c$ distributions are different for $R = 0.2$.

One more cross-check is to add and subtract the full systematic error range to the original histogram and calculate the binned p-value for these. Even with this extreme assumption of full positive correlation, the p-value for $p_T^{\mathrm{Cut}} > 0.2\,\mathrm{GeV}/c$ and R=0.2 stays below 1% while that for R=0.4 remains high.

Note well that these cross-checks are purely done to demonstrate the robustness of the physics message under extreme assumptions, they are not meant as realistic estimates of the p-value range.

4 Cross Checks

4.1 Negative A_J

For the original "hard core" di-jet selection with $p_T^{\rm Cut} > 2\,{\rm GeV}/c$, A_J is by construction positive. However, when the away-side jet recovers more energy than the original balance, A_J for matched dijets with soft constituents can become negative. During the GPC process, it was decided to change from the original presentation of $|A_J|$ to presenting the full range.

The original distribution using $|A_J|$ in Fig. 14 demonstrates that this choice does not obscure the physics conclusions. For $R = 0.4$, the Au+Au distribution is virtually indistinguishable from embedded p+p, while for $R = 0.2$, the distributions display significant differences.

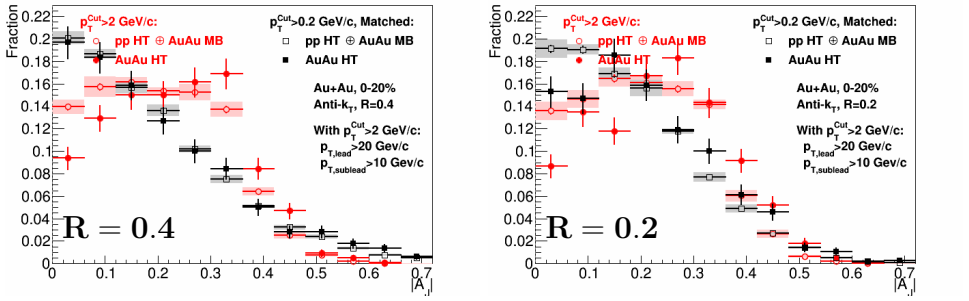

Figure 14: Distribution of $|A_J|$ (instead of A_J) for matched di-jets with $p_T^{\rm Cut} > 0.2\,{\rm GeV}/c$ and two different resolution parameters R.

4.2 Shift in A_J

It may be instructive to follow the balance restoration on a jet-by-jet basis using the quantity

$$\Delta A_J \equiv A_J(p_T^{\rm Cut} > 2\ {\rm GeV}/c) - A_J(p_T^{\rm Cut} > 0.2\ {\rm GeV}/c), \tag{8}$$

which can be interpreted as balance restored by soft constituents. These distributions are shown in Fig. 15. They are consistent with our conclusions, for $R = 0.4$ on average more balance is restored in Au+Au than in embedded p+p, while for $R = 0.2$ this difference is very small. However, in the current form this variable obscures more than it reveals. With more statistics, we plan future measurements of ΔA_J sliced in A_J bins, but will not include it into the paper at this point.

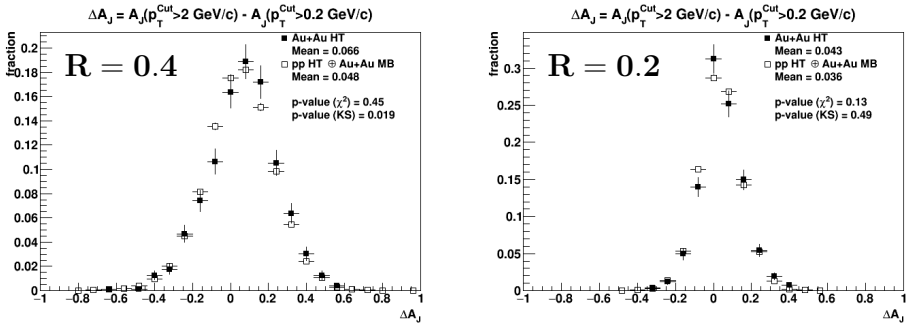

Figure 15: Distribution of ΔA_J for two different resolution parameters R .

4.3 Jet-hadron Correlation

A simple jet-track correlation with the leading and sub-leading jet, respectively, is shown in Fig. 16. No acceptance or any other correction is done for this cross-check, though the much more uniform jet axis distribution greatly alleviates the prominent sector boundary structure from a di-hadron correlation. This cross-check supports the observation that jet-like yield for hard-core di-jet pairs seems to be confined within $R = 0.4$.

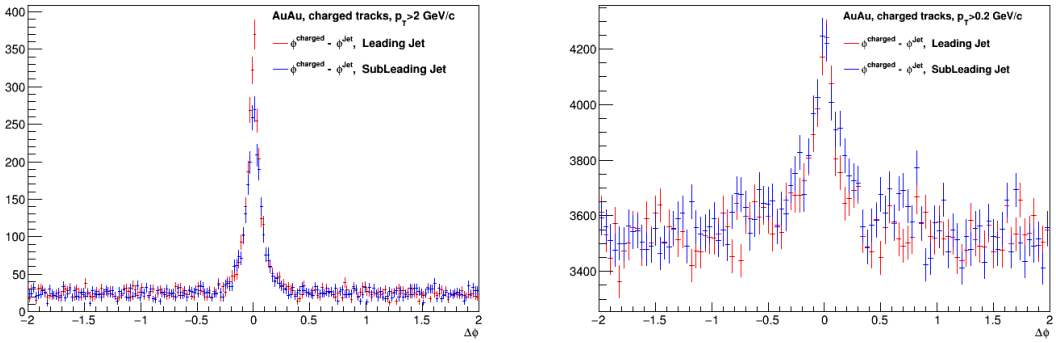

Figure 16: Jet-track correlations for $R = 0.4$.

4.4 Pythia Comparison

Fig. 17 shows the A_J analysis done on a high-statistics pure Pythia data set, without any smearing, inefficiencies, or heavy-ion background. They demonstrate the kinematic selection effect introduced by the constituent cut.

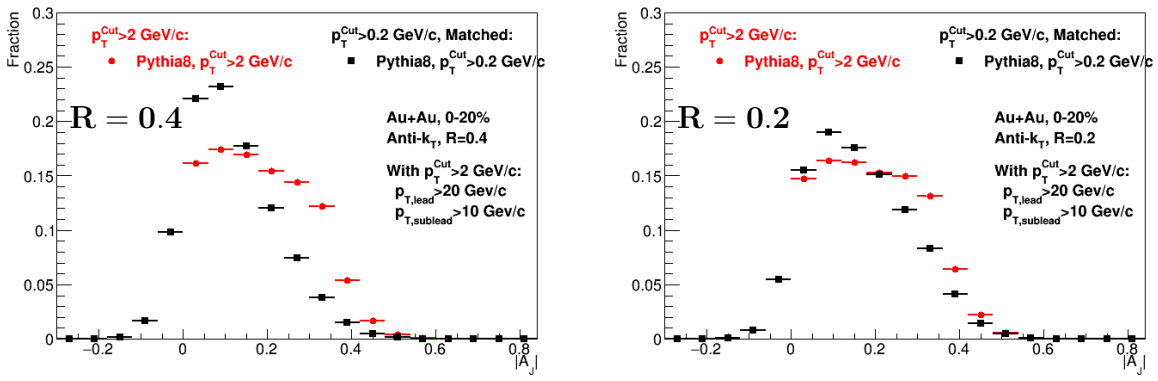

Figure 17: Distribution for matched di-jets in Pythia8 without background and with two different resolution parameters R.

4.5 Matching

During the geometric matching, a few of the original hard constituents may no longer be part of the jet found with softer constituents included. This number is very small, 51/960 leading, 71/960 sub-leading, only 4/960 di-jet pairs are affected on both sides. As shown in Fig. 18, even in those cases the overlap is still usually

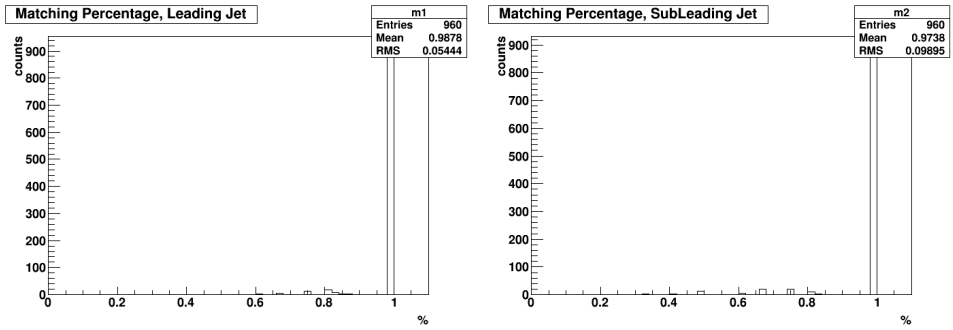

Figure 18: Percentage of original hard constituents retained in the matched jet for leading and sub-leading jets ($R = 0.4$).

between 60 and 80%. Further investigation shows that missing constituents are, as expected, usually close the 2 GeV/c and toward the edge of the jet cone. This is a small effect, and one that is present the same way in Au+Au and embedded p+p. Nevertheless, a comparison (done before the switchfrom displaying $|A_J|$ to displaying A_J) of Figure 1 done using the standard matching to the same plot rejecting jets that do not have 100% matching is shown in Fig. 19 as a cross-check. The resulting changes are minuscule and indeed affect Au+Au and embedded p+p identically.

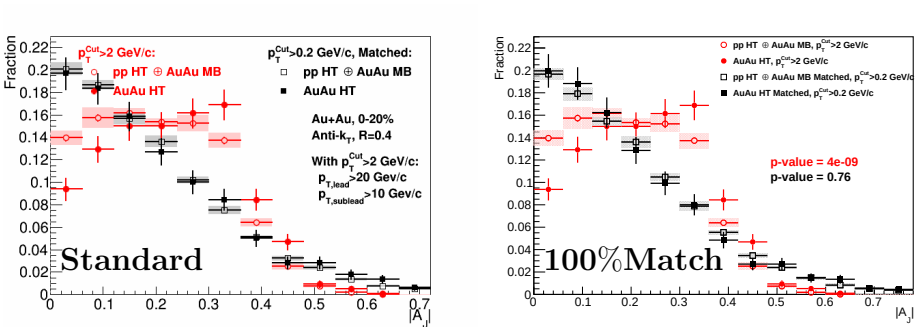

Figure 19: Distribution of $|A_J|$ for $R = 0.4$ using standard matching (left) and using only jets with 100% constituent matching (right).

References

[1] http://www.star.bnl.gov/protected/lfspectra/atimmins/AuAu200GeV/Centrality/page.html

[2] http://www.star.bnl.gov/protected/common/common2006/trigger2006/triggers2006.html

[3] http://www.star.bnl.gov/protected/common/common2007/trigger2007/triggers2007.html

[4] http://fastjet.fr

[5] http://fastjet.fr/repo/fastjet-doc-3.0.3.pdf

[6] https://drupal.star.bnl.gov/STAR/starnotes/private/psn0555

[7] ROOT TMath::KolmogorovTest, https://root.cern.ch/root/html534/TMath.html#TMath:KolmogorovTest

[8] A. Ohlsen (2013), *Investigating Parton Energy Loss with Jet-hadron Correlations and Jet vn at STAR* (Doctoral Dissertation) , https://drupal.star.bnl.gov/STAR/files/aohlson_thesis.pdf